Linear sweep voltammetry coupled to a quartz crystal microbalance for investigating the catalytic activity of the Mg(II)–water electrochemical system and managing the Mg oxy-hydroxide hydration state

Stéphanie Betelu, Romain Rodrigues, Alain Seron, Fabien Chauvet, Ioannis Ignatiadis, Théodore Tzedakis

Linear sweep voltammetry coupled to a quartz crystal microbalance for investigating the catalytic activity of the $Mg^{(II)}$–water electrochemical system and managing the Mg oxy-hydroxide hydration state

Stéphanie Betelu[a,*], Romain Rodrigues[a], Alain Seron[a], Fabien Chauvet[b], Ioannis Ignatiadis[a], Theodore Tzedakis[b]

[a] BRGM, 3 rue Claude Guillemin, F-45060 Orléans Cedex 02, France
[b] LGC, UMR-CNRS-5503. 118, Route de Narbonne, 31062 Toulouse Cedex 9, France

A B S T R A C T

This study provides an insight into the catalytic activity of the $Mg^{(II)}$–water electrochemical system, from aqueous magnesium chloride hexa-hydrate to magnesium oxy-hydroxide electro-nucleation, growth and evolution, using Linear Sweep Voltammetry (LSV) coupled to a Quartz Crystal Microbalance (QCM) ($-0.80 > E_{V/SCE} > -1.80$).

Interfacial phenomena occur at the gold resonator during cathodic polarization ($-0.90 > E_{V/SCE} > -1.80$).

$$Mg(H_2O)_6^{2+} \xrightarrow{-0.90>E_{V/SCE}>-1.25} Mg(H_2O)_4(OH)_2$$
$$\xrightarrow{-1.25>E_{V/SCE}>-1.50} Mg(H_2O)_2(OH)_2 \xrightarrow{-1.50>E_{V/SCE}>-1.70} Mg(OH)_2$$

From -0.90 V, reduction of the intramolecular water of the hexa-coordinated $Mg(H_2O)_6^{2+}$ cluster enhanced the cathodic current $i^{\circ}_{Mg(H_2O)_6^{2+}}/i^{\circ}_{(H_2O)}$. In the range $-1.25 > E_{V/SCE} > -1.70$, electrosynthesis of $Mg(H_2O)_4(OH)_2$ and its simultaneous gradual dehydration to $Mg(OH)_2$ take place. At lower potentials, experiments suggest intramolecular dehydroxylation of $Mg(OH)_2$ to MgO. The applied potential thus allows fine control of the hydration state of the Mg oxy-hydroxide.

1. Introduction

Magnesium-based materials are used for industrial and environmental applications [1–13]. Specifically, Mg and its alloys are of interest for energy-storage applications [14–20] due to their high volumetric capacities. In the case of Mg corrosion (spontaneous and/or under polarization), Mg displays a so-called "negative difference effect" that is clearly demonstrated under anodic polarization: the hydrogen evolution on the $Mg^{(0)}$ anode increases with increased current or potential (i.e. the water reduction rate increases with increasing the $Mg^{(0)}$ dissolution rate) [21–26]. By careful experimental design [24–27] and DFT calculations [25,27,28], several authors have shown that hydrated dissolution products (Mg oxy-hydroxides formed on the $Mg^{(0)}$ surface) catalyze hydrogen evolution; i.e. the chemical reduction of water (by galvanic corrosion of $Mg^{(0)}$) is energetically more favourable on a partially hydroxylated Mg surface than on $Mg^{(0)}$ [29]. The investigation on the electrochemical behaviour of Mg oxy-hydroxides is thus of primary importance for improving corrosion resistance and developing high-performance systems. In the same way, MgO and $(Mg(OH)_2)$-like compounds have attracted significant interest for industrial applications [30–39]. Various studies [40–45] claim that $Mg(OH)_2$-like compounds were electro-synthesized on platinum cathodes at fixed potential in the presence of compounds whose reduction produces OH^- (H_2O, O_2 or NO_3^- essentially), but no mechanism was proposed [46,47]. The acquisition of better insight into this process is among the objectives of our work, of which the first step is the study of the electrosynthesis pathway of $Mg(OH)_2$, the prototypical hydroxide phase.

In aqueous solution $Mg^{(II)}$ exists as a water-hexa-coordinated cluster $Mg(H_2O)_6^{2+}$ [48–51], whose structure is unaffected by counter ions (even Cl^-) [49], suggesting great stability. This octahedral magnesium complex behaves as a "weak Bronsted acid" Eq. (1).

$$Mg(H_2O)_6^{2+}{}_{(aq)} + H_2O_{(l)} \rightleftarrows Mg(H_2O)_5OH^{+}{}_{(aq)} + H_3O^{+}{}_{(aq)} \qquad pK = 11.2\ [48,51-53] \quad (1)$$

Besides the deprotonation of one water molecule, the resulting structure keeps its octahedral geometry, 'five waters' and the OH group bonding to the central atom in the first solvation shell [48,50–55]. In addition, $Mg^{(II)}$ keeps its octahedral coordination whatever the hydration state [48–55].

Our work aims at better understanding of the evolution of $Mg(H_2O)_6^{2+}$, under continuous sweeping of the applied potential. Using Linear Sweep Voltammetry (LSV) coupled to a Quartz Crystal Microbalance (QCM) provides insight into the electrochemical behaviour of the catalytic activity of the $Mg^{(II)}$–water electrochemical system and particularly the electro-nucleation, growth and evolution of magnesium oxy-hydroxides (i.e. Mg oxy-hydroxide hydration state management).

2. Materials and methods

2.1. Chemicals

Chemicals (normapurs > 99.8%) were supplied by Sigma-Aldrich. Experiments used $MgCl_2$, $6H_2O$ (2×10^{-2} M). They were conducted in NaCl 0.1 M (pH 5.5) milli-Q water (18.2 MΩ·cm).

2.2. Apparatus and techniques

Potentials were measured versus a saturated calomel electrode (SCE). Investigations were carried out under LSV (from −0.8 to −1.8 V, 5 mV·s^{-1} using a PAR-2273) coupled with QCM (QCM922 WinEchem Seiko EG & G, Freq. out: 20 kHz). QCM measurements were done on gold resonators (SCI-QA-A9M-Au(M)-25, AMETEK, 0.2 cm^2) also used as working electrodes. Experiments were conducted at 25 °C, in a divided cell. Both compartments were continuously stirred and deaerated (humidified N_2, 99.99999%, 1 bar). The platinum-wire counter electrode was immersed in NaCl 0.1 M and separated from the working-electrode compartment by a glass frit.

2.3. Methodology used for data processing

We logarithmically analysed (Tafel law, $I = I^{\circ}\exp(-\beta_c nF\eta/RT)$) current flow through the resonator versus E for the $I = f(E)$ data acquired in NaCl (0.1 M) and in $Mg(H_2O)_6^{2+}$ (2×10^{-2} M), NaCl (0.1 M), for comparison of the kinetic parameters (i°, β_c) of the involved redox systems. Equation $\Delta_R G^{\circ} = -RT\ln K_{eq} = -nFE$ served to evaluate the equilibrium constant K_{eq} of the involved reaction.

We calculated the resonator mass variation with the Sauerbrey relation [56]. We then calculated the number of moles (A) of the solid (κ) generated during electrolysis using Eq. (2):

$$\text{produced flux of } \kappa = dA/dt = yFI_{(t)}/nF \sim \Delta A/\Delta t \quad (2)$$

Numerical integration of $I = f(E)$ curves provided the instantaneous (A_i^{inst}) number of moles of κ electro-synthesized during time interval $\Delta t = t_{i+1} - t_i$ Eq. (3), as well as its cumulative number of moles (A_i^c) at time t_i Eq. (4):

$$A^{inst}{}_{(i+1)} = (I_{i+1} + I_i) \times 0.5 \times \Delta t/(n \times F) \quad (3)$$

where Δt represents the time step (0.2 s) from −0.8 V ($t = 0$) to −1.8 V ($t = 280$ s). The cumulative number of moles of κ (A_i^c) was calculated as Eq. (4):

$$A^c{}_i = \Sigma_{i=1}^{i} A^{inst}{}_i \quad (4)$$

Comparison of this number of moles with that obtained from the mass measured by QCM, led to proposing a formula for the coating on the resonator.

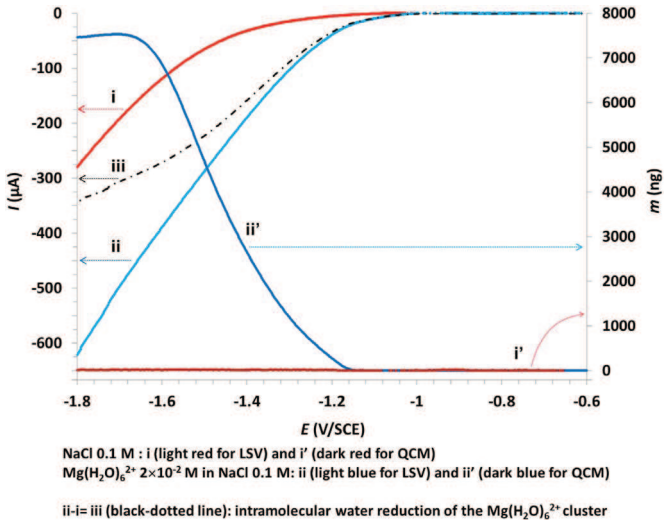

Fig. 1. Coupled LSV (left axis, curves i and ii) and QCM (right axis, curves i' and ii') measurements. Curve iii was obtained by subtracting curve ii from curve i.

3. Results and discussion

3.1. Voltammetric behaviour of $Mg(H_2O)_6^{2+}$ and simultaneous monitoring of cathode mass-variation

Fig. 1 presents the voltammograms $I = f(E)$ and the associated mass-variation curves for the following cases:

- i and i': 0.1 M NaCl,
- ii and ii': 2×10^{-2} M $Mg(H_2O)_6^{2+}$, NaCl (0.1 M)

3.1.1. The residual current

Fig. 1,i shows the current-potential curve obtained from NaCl. Due to the high overvoltage, the effective reduction of H_2O on gold begins at −1.03 V. The current is exponentially shaped reflecting the activation limitation of water reduction according to Eq. (5):

$$H_2O + e^- \rightarrow \tfrac{1}{2}H_2 + OH^-,\ E_{I\neq 0} = (-0.830 - 0.059 \times pH) + \eta \quad (5)$$

Logarithmic analysis of the $I = f(E)$ curve leads to Eq. (6) that leads to: a) the value of the cathodic electronic transfer coefficient ($\beta_c = 0.20$, assuming $n = 1$ e^-/mol of reduced water), and b) the exchange current density $i^{\circ}{}_{H_2O} = 2.29 \times 10^{-9}$ A·cm^{-2}, which clearly translates an irreversible redox system:

$$\ln(I_{(A)}) = -21.505 - 7.950 \times E_{V/SCE},\ R^2 = 0.9998,\ -1.30 > E_{V/SCE} > -1.60 \text{ and } E_{i=0} = -1.03 \text{ V} \quad (6)$$

Fig. 1,i' clearly shows the absence of any solid deposition on the resonator.

3.1.2. Magnesium chloride

Fig. 1,ii shows the cathodic behaviour of $Mg(H_2O)_6^{2+}$. The exponentially shaped $I = f(E)$ curve shows a higher current magnitude compared with that obtained in NaCl (Fig. 1,i). Also, effective reduction begins at −0.902 V instead of −1.03 V in NaCl. Logarithmic evolution of $I = f(E)$ shows a linear segment (until −1.50 V) (Eq. (7)) that helps determining the kinetic parameters of the redox system:

$$i^{\circ}{}_{Mg(H_2O)_6}{}^{2+} = 1.32 \times 10^{-6} \text{A·cm}^{-2} \text{ and } \beta_c n = 0.12.$$
$$\ln(I_{(A)}) = -15.150 - 4.720 \times E_{V/SCE},\ R^2 = 0.9988,$$
$$E_{V/SCE} > -1 \text{ and } E_{i=0} = -0.902 \text{ V} \quad (7)$$

The increased exchange-current density (i.e. $i^{\circ}{}_{Mg(H_2O)_6^{2+}}/i^{\circ}{}_{(H_2O)} = 575$) shows that the involved redox system is less

irreversible than the direct reduction of H_2O. Moreover, $\beta_c \times n = 0.12$ is approximately half of that obtained from a NaCl solution ($\beta_c \times 1 = 0.20$). Subtraction of the residual current (Fig. 1,i from Fig. 1,ii) determines the net current related to the presence of Mg $(H_2O)_6^{2+}$ (Fig. 1,iii), showing a pseudo-plateau corresponding to mass-transfer limitation.

The mass variation of the resonator obtained by the QCM (Fig. 1,ii') can be separated into various areas. For potentials over ~ − 1.2 V, the mass deposited at the resonator is quasi nil, even if the current increases from 0 to 25 μA (Fig. 1,ii). For potentials more cathodic than ~ − 1.2 V, the mass gain is sharply enhanced and reaches a maximum value of ~7.5 μg at ~ − 1.7 V, revealing the rapid growth of a coating at the interface. From − 1.7 V to − 1.8 V, the mass-variation curve (Fig. 1,ii') shows a slightly decreasing pseudo-plateau, whereas the cathodic reduction current further increases.

3.2. Discussion

The increase in current magnitude from − 0.9 V to − 1.15 V suggests the existence of an electroactive species different from free water. The concomitant increase of resonator mass from − 1.15 to − 1.7 V suggests that the electro-synthesized solid (named κ) is non-passivating as it allows simultaneous coating growth and current flow.

As $Mg^{(II)}$ is electro-inactive under the chosen conditions [57], the observed current is attributed to the reduction of intramolecular water of a $Mg(H_2O)_6^{2+}$ cluster according to Eq. (8):

$$Mg(H_2O)_6^{2+} + \xi\, e^- \rightarrow \xi/2\, H_{2(g)} + Mg(H_2O)_\lambda(OH)_\xi^{(2-\xi)+} \quad (8)$$

The only species at low concentration that explains the obtained limiting current (Fig. 1,iii) is $Mg(H_2O)_6^{2+}$. This agrees with the enhancement of exchange-current density recorded in $Mg(H_2O)_6^{2+}$ $i^\circ_{Mg(H_2O)_6^{2+}}/i^\circ_{(H_2O)} = 575$). This is also consistent with $Mg^{(II)}$ octahedral geometry.

The electro-generated compound is written as Mg $(H_2O)_\lambda(OH)_\xi^{(2-\xi)+}$, where λ is the hydration state, and ξ, the number of hydroxyl groups per cluster:

- ξ = 0, the initial hexa-hydrated magnesium is $Mg(H_2O)_6^{2+}$;
- ξ = 1, the compound $[Mg(H_2O)_5(OH)]^+$ is dissolved;
- ξ = 2, the compound $[Mg(H_2O)_\lambda(OH)_2]$, called κ, is in solid form.

To obtain an electro-synthesized coating, ξ must be 2; thus the first possible cluster that can precipitate is $Mg(H_2O)_4(OH)_2$ also implying 2 electrons exchanged in Eq. (8).

For a better understanding of the concomitant phenomena observed at the resonator, the interfacial pH was estimated from Fig. 1,i using the Leveque equation and the Nernst-film model; pH reaches ~10.1 at − 1.15 V (Fig. 2,i), creating favourable conditions for brucite precipitation. It then continuously increases in the range 10.4–12.1 with the potential decreasing from − 1.2 V to − 1.8 V.

The mass of κ obtained from QCM versus *E* (Fig. 1,ii'), enables estimating the coating growth rate ($\Delta m/\Delta t$); its evolution (Fig. 2,ii) is correlated with the λ values (Fig. 2,iii and Fig. 2,iv). The mass *m* of the electrodeposit obtained from QCM during a time interval (*i* to *i* + 1) versus *E*, is expressed for this interval by Eq. (9):

$$\Delta m_{(i\ to\ i+1)} = A^{ins}_{(i+1)} \times [M_{(Mg)} + \lambda_{(i+1)} \times M_{(H_2O)} + 2 \times M_{(HO)}] \quad (9)$$

where $A^{inst}_{(i+1)}$ is the instantaneous number of κ moles defined in Eq. (3) using one electron per intramolecular reduced water. The calculation of $A^{inst}_{(i+1)}$ requires the net current used for reduction of the magnesium hexa-hydrated complex, obtained by subtracting Fig. 1,i from Fig. 1,ii. The resulting net current (Fig. 1,iii) was assumed to correspond to reduction of the intramolecular water of $Mg(H_2O)_6^{2+}$ (faradic yield *y*F = 1). Using data from Fig. 1,iii and Fig. 1,ii', Eq. (9) determines the instantaneous value of $\lambda_{(i+1)}$ for time interval *i* to *i* + 1. Fig. 2,iii gives

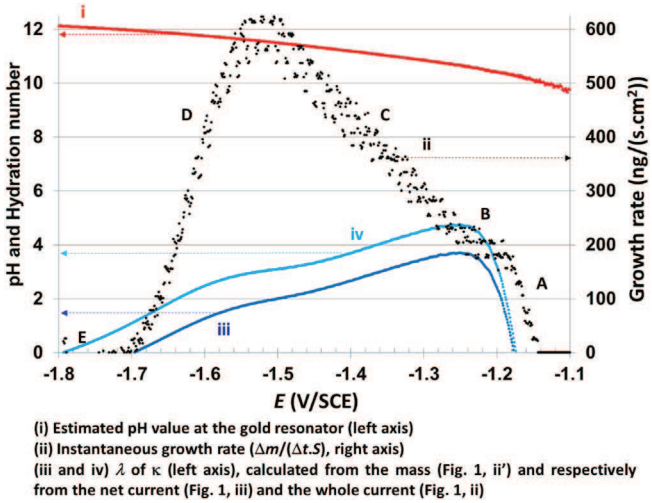

Fig. 2. Applied potential dependency on i: the pH, ii: the instantaneous growth rate as well as iii and iv: the evolution of $Mg(OH)_2$ hydration state (λ).

the corresponding λ versus *E*. For better comparison, Fig. 2,iv shows the λ = f(*E*) results calculated using the whole cathodic current (i.e. using Fig. 1,ii and Fig. 1,ii').

Fig. 2,ii can be divided into five segments, A) − 1.15 V to − 1.18 V, B) − 1.18 V to − 1.25 V, C) − 1.25 V to − 1.5 V, D) − 1.5 V to − 1.7 V and E) − 1.7 V to − 1.8 V. Until − 1.15 V, the current magnitude increases without depositing mass at the resonator. Reduction of a) free water (Eq. (5)) and b) part of intramolecular water of the $Mg(H_2O)_6^{2+}$ cluster (Eq. (8)) occurs, but no solid precipitates. Deposition starts in segment A ($-1.15 > E_{V/SCE} > -1.18$), in agreement with the pH reached at the electrode (10.1–10.4). The growth rate curve shows a linear increase from 0 to 180 ng/(s·cm²).

At − 1.25 V, Fig. 2,iii and Fig. 2,iv indicate a hydration state of four ($3.5 < \lambda < 4.5$) for adduct κ precipitation, confirming (Eq. (8)) with ξ = 2 and the precipitation of octahedral $Mg(H_2O)_4(OH)_2$. Considering a) 2×10^{15} atoms of Au per cm² [58], b) the number of moles of electro-synthesized κ, and c) the resonator area, we deduced that the number of $Mg(H_2O)_4(OH)_2$ monomeric units coated at the resonator reaches ~8 per gold atom at − 1.25 V.

To estimate the thermodynamic stability of $Mg(H_2O)_4(OH)_2$ [formed by Eq. (8), ξ = 2], the equilibrium constant of its formation was calculated according to Eq. (10).

$$Mg(H_2O)_6^{2+} + 2\, OH^- \rightleftarrows Mg(H_2O)_4(OH)_{2(s)} + 2\, H_2O \quad (10)$$

Reaction (10) can be obtained by subtracting twice Eqs. (5) from (8), where ξ = 2, or $\Delta_{R10}G^\circ = \Delta_{R8}G^\circ - 2\Delta_{R5}G^\circ - RT\ln K_{R10} = (-n_{R8}FE^\circ_{R8}) - 2(-n_{R5}FE^\circ_{R5})$.

To obtain a rough estimate of K_{R10}, the potential of both Eqs. (5) and (8) was piqued at the *I* = f(*E*) curves for a given current value: a typical set of values is $E_{(i=0)free\ H2O} = -1.03$ V; $E_{(i=0)Mg(H2O)6^{2+}} = -0.902$ V, giving $K_{R10} = 2.1 \times 10^4$ ($\Delta_{R10}G^\circ = -5.9$ kcal.mol^{-1}). Though the determination of this constant is not rigorous, $Mg(H_2O)_4(OH)_2$ appears relatively stable. During the formation of $Mg(H_2O)_4(OH)_2$, the growth rate is constant (180 ng/(s·cm²)) until reaching complete coverage of the working electrode by tetra-hydrated magnesium hydroxide (*E* = − 1.25 V, segment B in Fig. 2,ii).

From − 1.25 V to − 1.5 V (segment C, Fig. 2,ii), the following points should be mentioned: a) the mass of the solid deposit increases; b) the growth rate shows an almost linear increase (from ~220 to ~620 ng/(s·cm²)); and c) the hydration state λ of the coating decreases continuously until reaching ~2. This increase of the solid-deposit mass means that formation of $Mg(H_2O)_4(OH)_2$ occurs as in Eq. (8), but also that the hexa-coordinated cluster dehydrates, in agreement with the λ value and according to Eq. (11):

$$Mg(H_2O)_4(OH)_{2(s)} + 2\,e^- \rightarrow Mg(H_2O)_2(OH)_{2(s)} + H_{2(g)} + 2\,OH^- \quad (11)$$

A competitive process thus occurs at the electrode, between the electro-generation of $Mg(H_2O)_4(OH)_2$ and its gradual dehydration to $Mg(H_2O)_2(OH)_2$. The coating growth rate has a maximum value of 620 ng/(s·cm^2) at ~ − 1.5 V. Beyond − 1.55 V (segment D), both the coating growth rate and λ decrease and cancel (both become 0) at a potential of ~ − 1.7 V. During this period, both current (Fig. 1,ii) and mass of the coating (Fig. 1,ii') increase.

As before, these facts indicate another competitive process occurring at the resonator. Because the coating mass increases, it can be concluded that new $Mg(H_2O)_4(OH)_2$ precipitates, while some dehydrates sequentially Eqs. (11) and (12) until $Mg(OH)_2$.

$$Mg(H_2O)_2(OH)_{2(s)} + 2\,e^- \rightarrow Mg(OH)_{2(s)} + H_{2(g)} + 2\,OH^- \quad (12)$$

In fact, the solid coating consists of a mix of three compounds: $Mg(H_2O)_4(OH)_2$, $Mg(H_2O)_2(OH)_2$ and $Mg(OH)_2$. The pseudo-plateau observed for λ at − 1.5 V indicates an energy gap limiting the total dehydration process. Our data show that, at − 1.7 V, the overall composition reaches $Mg(OH)_2$ and the number of monomeric $Mg(OH)_2$ units is 200 per gold atom. In agreement with Vaiss et al. [59], who mention a 90° O-Mg-O angle and an Mg-O distance of 2.1 Å, the coating thickness reaches ~30 nm.

At this stage, deposition of new $Mg(H_2O)_4(OH)_2$ stops; the solid $Mg(OH)_2$ coating prevents the diffusion of new $Mg(H_2O)_6^{2+}$ clusters to the gold electrode. Nevertheless, beyond − 1.7 V, reduction continues (Fig. 1,ii) and the current is more than twice that obtained in the absence of $Mg(H_2O)_6^{2+}$ (Fig. 1,i). In addition, Eqs. (11) and (12) release hydroxyl ions that basify the interfacial area and slow-down the water-reduction reaction. This appears to be in complete disagreement with the observed current magnitude, especially since the mass simultaneously shows a slight decrease (Fig. 1,ii') from − 1.7 V. A plausible explanation of the current increase beyond − 1.7 V is an intramolecular dehydroxylation of $Mg(OH)_2$ to magnesium oxide (Eq. (13)), the subject of a future study.

$$Mg(OH)_{2(s)} + e^- \rightarrow MgO_{(s)} + ½\,H_{2(g)} + OH^- \quad (13)$$

4. Conclusions

This work aimed at investigating and improving the knowledge of the catalytic activity of the $Mg^{(II)}$-water electrochemical system and particularly the Mg-oxyhydroxides electro-nucleation, growth and evolution, using coupled LSV-QCM methods. The work was done in NaCl, using a gold resonator via water reduction to hydrogen in the absence and presence of $Mg(H_2O)_6^{2+}$. Coupled current and mass data indicate that the:

a) Intramolecular water of the $Mg(H_2O)_6^{2+}$ clusters is reduced (− 0.902 V/SCE), thus enhancing the current in comparison with the data acquired in NaCl;
b) Precipitation of a hexa-coordinated compound, $Mg(H_2O)_4(OH)_2$ occurs from cathodic potentials over − 1.2 V/SCE;
c) Value of the Gibbs free enthalpy variation of the formation reaction of such brucite (Eq. (10)) is negative, indicating a certain stability of this electro-synthesized hexa-coordinated compound.

Beyond − 1.25 V/SCE, a competitive process occurs at the resonator, between the electro-generation of $Mg(H_2O)_4(OH)_2$ and its gradual dehydration to a) to $Mg(H_2O)_2(OH)_2$ from − 1.25 V/SCE to − 1.5 V/SCE, and b) to $Mg(OH)_2$ from − 1.5 V/SCE to − 1.7 V/SCE. The $Mg(OH)_2$ electro-synthesized coating is ~30 nm thick at − 1.7 V/SCE. From − 1.7 V/SCE to − 1.8 V/SCE, both current and mass magnitude indicate $Mg(OH)_2$ dehydroxylation. MgO is the presumed product.

Our results provide a suitable tool for fine control of Mg oxy-hydroxide hydration state.

This work is the first key step for a better insight in the electrochemical behaviour of the $Mg^{(II)}$-water electrochemical system. Further experiments should be conducted by using electrochemical and synchrotron coupling for a better insight in the attendant atomic-scale phenomena.

Acknowledgments

This work was funded by BRGM: QCMB-E:2014. Dr. H.M. Kluijver corrected the English version. The authors thank the anonymous reviewer for suggesting constructive improvements via his enthusiastic comments.

References

[1] I.J. Polmear, Light Alloys: From Traditional Alloys to Nanocrystals, 4th edn, Butterworth-Heinemann, Oxford, 2005.
[2] D.J. Cuscueta, M. Melnichuk, H.A. Peretti, H.R. Salva, A.A. Ghilarducci, Magnesium influence in the electrochemical properties of La–Ni base alloy for Ni–MH batteries, Int. J. Hydrog. Energy 33 (2008) 3566–3570.
[3] M. Shinohara, E. Araki, M. Mochizuki, T. Kanazawa, K. Suyehiro, Practical application of a sea-water battery in deep-sea basin and its performance, J. Power Sources 187 (2009) 253–260.
[4] Ø. Hasvold, T. Lian, E. Haakaas, N. Størkersen, O. Perelman, S. Cordier, CLIPPER: a long-range, autonomous underwater vehicle using magnesium fuel and oxygen from the sea, J. Power Sources 136 (2004) 232–239.
[5] H. Zhao, P. Bian, D. Ju, Electrochemical performance of magnesium alloy and its application on the sea water battery, J. Environ. Sci. 21 (2009) S88–S91.
[6] N. Julkapli, S. Bagheri, Magnesium oxide as a heterogeneous catalyst support, Rev. Inorg. Chem. 36 (2015) 1–41.
[7] Y.H. Duan, D.C. Sorescu, CO_2 capture properties of alkaline earth metal oxides and hydroxides: a combined density functional theory and lattice phonon dynamics study, J. Chem. Phys. 133 (2010) 074508 (1 − 11).
[8] R.V. Siriwardane, R.W. Stevens Jr., Novel regenerable magnesium hydroxide sorbents for CO_2 capture at warm gas temperatures, Ind. Eng. Chem. Res. 48 (2009) 2135–2141.
[9] P.C. Lin, C.W. Huang, C.T. Hsiao, H. Teng, Magnesium hydroxide extracted from a magnesium-rich mineral for CO_2 sequestration in a gas–solid system, Environ. Sci. Technol. 42 (2008) 2748–2752.
[10] L. Shi, D.Q. Li, J.R. Wang, S.F. Li, D.G. Evans, X. Duan, Synthesis, flame-retardant and smoke-suppressant properties of a borate-intercalated layered double hydroxide, Clay Clay Miner. 53 (2005) 294–300.
[11] D. Jin, X. Gu, X. Yu, G. Ding, H. Zhu, K. Yao, Hydrothermal synthesis and characterization of hexagonal $Mg(OH)_2$ nano-flake as a flame retardant, Mater. Chem. Phys. 112 (2008) 962–965.
[12] F. Cavani, F. Trifiro, A. Vaccari, Hydrotalcite-type anionic clays: preparation, properties and applications, Catal. Today 11 (1991) 173–301.
[13] T.B. Abbott, Magnesium: Industrial and research developments over the last 15 years, Corros. Sci. 71 (2015) 120–127.
[14] Y. Orikasa, T. Masese, Y. Koyama, T. Mori, M. Hattori, K. Yamamoto, T. Okado, Z.D. Huang, T. Minato, C. Tassel, J. Kim, Y. Kobayashi, T. Abe, H. Kageyama, Y. Uchimoto, High energy density rechargeable magnesium battery using earth-abundant and non-toxic elements, Sci Rep 4 (2014) 5622 (1–6).
[15] M. Tsang, A. Armutlulu, A.W. Martinez, B. Allen, M.G. Allen, Biodegradable magnesium/iron batteries with polycaprolactone encapsulation: a microfabricated power source for transient implantable devices, Microsyst. Nanoeng. 1 (2015) 15024 (1 − 10).
[16] R. Van Noorden, The rechargeable revolution: a better battery, Nature 507 (2014) 26–28.
[17] C.B. Bucur, T. Gregory, A.G. Oliver, J. Muldoon, Confession of a magnesium battery, J. Phys. Chem. Lett. 6 (2015) 3578–3591.
[18] R. Mohtadi, F. Mizuno, Magnesium batteries: Current state of the art, issues and future perspectives, Beilstein J. Nanotechnol. 5 (2014) 1291–1311.
[19] L. Yin, X. Huang, H. Xu, Y. Zhang, J. Lam, J. Cheng, J.A. Rogers, Materials, designs, and operational characteristics for fully biodegradable primary batteries, Adv. Mater. 26 (2014) 3879–3884.
[20] S. Banerjee, C.G.S. Pillai, C. Majumder, First-principles study of the H_2 interaction with transition metal (Ti, V, Ni) doped Mg(0001) surface: implications for H-storage materials, J. Chem. Phys. 129 (2008) 174703–174706.
[21] M. Curioni, The behaviour of magnesium during free corrosion and potentiodynamic polarization investigated by real-time hydrogen measurement and optical imaging, Electrochim. Acta 120 (2014) 284–292.
[22] G.S. Frankel, A. Samaniego, N. Birbilis, Evolution of hydrogen at dissolving magnesium surfaces, Corros. Sci. 70 (2013) 104–111.
[23] G. Williams, N. Birbilis, H.N. McMurray, The source of hydrogen evolved from a magnesium anode, Electrochem. Commun. 36 (2013) 1–5.
[24] M. Taheri, J.R. Kish, N. Birbilis, M. Danaie, E.A. McNally, J.R. McDermid, Towards a physical description for the origin of enhanced catalytic activity of corroding magnesium surfaces, Electrochim. Acta 116 (2014) 396–403.
[25] S.H. Salleh, S. Thomas, J.A. Yuwono, K. Venkatesan, N. Birbilis, Enhanced hydrogen

evolution on $Mg(OH)_2$ covered Mg surfaces, Electrochim. Acta 161 (2015) 144–152.
[26] Z.P. Cano, M. Danaie, J.R. Kish, J.R. McDermid, G.A. Botton, G. Williams, Physical characterization of cathodically-activated corrosion filaments on magnesium alloy AZ31B, Corrosion 71 (2015) 146–159.
[27] K.S. Williams, V. Rodriguez-Santiago, J.W. Andzelm, Modeling reaction pathways for hydrogen evolution and water dissociation on magnesium, Electrochim. Acta 210 (2016) 261–270.
[28] J.A. Yuwono, N. Birbilis, K.S. Williams, N.V. Medhekar, Electrochemical stability of magnesium surfaces in an aqueous environment, J. Phys. Chem. C 120 (2016) 26922–26933.
[29] K.S. Williams, J.P. Labukas, V. Rodriguez-Santiago, J.W. Andzelm, First principles modeling of water dissociation on Mg(0001) and development of a Mg surface Pourbaix diagram, Corros. Sci. 71 (2015) 209–223.
[30] Q. Wang, D. O'Hare, Recent advances in the synthesis and application of layered double hydroxide (LDH) nanosheets, Chem. Rev. 112 (2012) 4124–4155.
[31] C. Mousty, F. Leroux, LDHs as electrode materials for electrochemical detection and energy storage: supercapacitor, battery and (bio)-sensor, Recent Pat. Nanotechnol. 6 (2012) 174–192.
[32] M.F. Shao, R.K. Zhang, Z.H. Li, M. Wei, D.G. Evans, X. Duan, Layered double hydroxides toward electrochemical energy storage and conversion: design, synthesis and applications, Chem. Commun. 51 (2015) 15880–15893.
[33] J. Wang, L. Wang, X. Chen, Y. Lu, W. Yang, Chemical power source based on layered double hydroxides, J. Solid State Electrochem. 19 (2015) 1933–1948.
[34] P. Grubel, K.R. Bhaskar, D.R. Cave, P. Garik, H.E. Stanley, J.T. Lamont, Interaction of an aluminium-magnesium-containing antacid and gastric mucous: possible contribution to the cytoprotective function of antacids, Aliment. Pharmacol. Ther. 11 (1997) 139–145.
[35] M. del Arco, S. Gutierrez, C. Martın, V. Rives, J. Rocha, Synthesis and characterization of layered double hydroxides (LDH) intercalated with non-steroidal anti-inflammatory drugs, J. Solid State Chem. 177 (2004) 3954–3962.
[36] A. Ookubo, K. Ooi, H. Hayashi, Hydrotalcites as potential adsorbents of intestinal phosphate, J. Pharm. Sci. 81 (1992) 1139–1140.
[37] B. Li, J. He, D.G. Evans, X. Duan, Inorganic layered double hydroxides as a drug delivery system-intercalation and in vitro release of fenbufen, Appl. Clay Sci. 27 (2004) 199–207.
[38] C. Mousty, Sensors and biosensors based on clay-modified electrodes — new trends, Appl. Clay Sci. 27 (2004) 159–177.
[39] C. Taviot-Guého, P. Vialat, F. Leroux, F. Razzaghi, P. Perrot, O. Sel, N. Daugaard Jensen, U. Gro Nielsen, S. Peulon, E. Elkaim, C. Mousty, Dynamic characterization of inter- and intralamellar domains of cobalt-based layered double hydroxides upon electrochemical oxidation, Chem. Mater. 28 (2016) 7793–7806.
[40] G.H.A. Therese, P.V.J. Kamath, Cathodic reduction of different metal salt solutions Part I: synthesis of metal hydroxides by electrogeneration of base, J. Appl. Electrochem. 28 (1998) 539–543.
[41] G.H.A. Therese, P.V.J. Kamath, Electrochemical synthesis of metal oxides and hydroxides, Chem. Mater. 12 (2000) 1195–1204.
[42] F. Wu, J. Liang, W. Li, Electrochemical deposition of $Mg(OH)_2$/GO composite films for corrosion protection of magnesium alloys, J. Magnesium Alloys 3 (2015) 231–236.
[43] I. Gualandi, M. Monti, E. Scavetta, D. Tonelli, V. Prevot, C. Mousty, Electrodeposition of layered double hydroxides on platinum: insights into the reactions sequence, Electrochim. Acta 152 (2015) 75–83.
[44] L. Indira, P.V. Kamath, Electrogeneration of base by cathodic reduction of anions: novel one-step route to unary and layered double hydroxides (LDHs), J. Mater. Chem. 4 (1994) 1487–1490.
[45] M. Monti, P. Benito, F. Basile, G. Fornasari, M. Gazzano, E. Scavetta, D. Tonelli, A. Vaccari, Electrosynthesis of Ni/Al and Mg/Al layered double hydroxides on Pt and FeCr alloy supports: study and control of the pH near the electrode surface, Electrochim. Acta 108 (2013) 596–604.
[46] J.L. Warren, T.H. Geballe, Research opportunities in new energy-related materials, Mater. Sci. Eng. 50 (1981) 149–198.
[47] C.N.R. Rao, Chemical synthesis of solid inorganic materials, Mater. Sci. Eng. B18 (1993) 1–21.
[48] V.E. Jackson, A.R. Felmy, D.A. Dixon, Prediction of the p*K*a's of aqueous metal ion + 2 complexes, J. Phys. Chem. A 119 (2015) 2926–2939.
[49] R. Caminiti, G. Licheri, G. Piccaluga, G. Pinna, Diffraction of X-rays and hydration phenomena in aqueous solutions of $Mg(NO_3)_2$, Chem. Phys. Lett. 61 (1979) 45–49.
[50] W. Bol, G.J.A. Gerrits, C.L. van Panthaleon Eck, The hydration of divalent cations in aqueous solution. An X-Ray investigation with isomorphous replacement, J. Appl. Crystallogr. 3 (1970) 486– – 492.
[51] L. Bernasconi, E.J. Baerends, M. Sprik, Long-range solvent effects on the orbital interaction mechanism of water acidity enhancement in metal ion solutions: a comparative study of the electronic structure of aqueous Mg and Zn dications, J. Phys. Chem. B 110 (2006) 11444–11453.
[52] J.L. Adcock, Teaching Bronsted–Lowry acid–base theory in a direct comprehensive way, J. Chem. Educ. 78 (2001) 1495–1496.
[53] S.J. Hawkes, All positive ions give acid solutions in water, J. Chem. Educ. 73 (1996) 516–517.
[54] W. Grzybkowski, Nature and properties of metal cations in aqueous solutions, Pol. J. Environ. Stud. 15 (2006) 655–663.
[55] A.D. Becke, Density-functional thermochemistry. III, The role of exact exchange, J. Chem. Phys. 98 (1993) 5648– – 5652.
[56] G. Sauerbrey, Verwendung von schwingquarzen zur wagung dunner schichten und zur mikrowagung, Z. Physik. 155 (1959) 206–222.
[57] P. Vany'sek, Electrochemical Series in Handbook of Chemistry and Physics, CRC Press, Boca Raton, 1986.
[58] P.C. Lee, D. Meisel, Adsorption and surface-enhanced Raman of dyes on silver and gold sols, J. Phys. Chem. 86 (1982) 3391–3395.
[59] V.S. Vaiss, I. Borges Jr., F. Wypych, A.A. Leitão, Formation reaction mechanisms of hydroxide anions from $Mg(OH)_2$ layers, Chem. Phys. 418 (2013) 1–7.